Impact Cratering and Spall Failure of Gabbro

by

Manfred A. Lange*

Thomas J. Ahrens

and

Mark B. Boslough

Seismological Laboratory, 252-21

California Institute of Technology

Pasadena, California 91125

1983

*Now at: Alfred-Wegener Institute for Polar Research

Columbus Center

D2850 BREMERHAVEN

Federal Republic of Germany

Abstract

Both hypervelocity impact and dynamic spall experiments were carried out on a series of well-indurated samples of gabbro. The impact experiments carried out with 0.04 to 0.2g, 5-6 km/sec projectiles produced deci-centimeter-sized craters and demonstrated crater efficiencies of 6×10^{-9} g/erg, an order of magnitude greater than in metal and some two to three times that of previous experiments on less strong igneous rocks. Most of the crater volume (some 60 to 80%) is due to spall failure. Distribution of cumulative fragment number, as a function of mass of fragments with masses greater than 0.1 gram yield values of $b = d(\log_{10} N_f)/d\log_{10}(m)$ of -0.5 to -0.6, where N_f is the cumulate number of fragments and m is the mass of fragments. These values are in agreement or slightly higher than those obtained for less strong rocks and indicate that a large fraction of the ejecta resides in a few large fragments. The large fragments are plate-like with mean values of B/A and C/A of 0.8 and 0.2 respectively (A = long, B = intermediate, and C = short fragment axes). The small fragments (with mass $<$ 0.1g and B $\sim$ 0.1 mm) represent material which has been subjected to shear failure. The dynamic tensile strength of San Marcos gabbro was determined at strain rates of 10^4 to 10^5 sec^{-1} to be 147 $\pm$ 9 Mpa. This is 3 to 10 times greater than inferred from quasi-static (strain rate 10^0 sec^{-1}) loading experiments. Utilizing these parameters in a continuum fracture model predicts tensile strength of $\sigma_m \propto \dot{\varepsilon}^{[0.25-0.3]}$, where $\dot{\varepsilon}$ is strain rate. We correlate the high dynamic tensile strength with the high value of cratering efficiency. We suggest that the high spall strength

of basic igneous rocks gives rise to enhanced cratering efficiencies in the $< 10^2$ m crater diameter strength-dominated regime. This enhanced mechanism would improve the efficiency of proposed impact mechanisms for removing basic rocks from the surfaces of planets such as the moon or Mars.

1. Introduction

The size and shape of impact and explosion craters having characteristic dimensions of less than $\lesssim 10^2$ meters are strongly dependent on the dynamic strengths of the rock target medium and the impactor properties and speed. The size and velocity distribution of fragments in the resulting ejecta cloud also depend on these same dynamic strength characteristics of the target (Grady and Kipp, 1980; Melosh, 1983). Morreoveer, the recent discovery of lightly shocked meteorites, which apparently represent impact ejecta from the moon's (and posssibly Mars) surface have focused considerable interest on the spall phenomena as it occurs on planetary surfaces (Wasson and Wetherill, 1979; Stolper et al., 1979; Wood and Ashwal, 1980; Melosh, 1983). Also, the possible destruction of growing protoplanets by impacting planetesimals is determined by the ability of the cratered planet to withstand dynamic stresses associated with impact.

Attempts to generalize the description of fracturing and comminution processes and to obtain predictive capability for practical applications of breakage have been recently summarized by Grady and Kipp, 1980; Shockey et al., 1979; and Curran et al., 1978. They have described dynamic tensile failure by providing numerical models which consider both the statistical and microscopic aspects of nucleation and growth of cracks under the influence of varying strain rates. These models yield results which are in qualitative agreement with a given set of data for a rock type. They are not qualitatively predictive, however, in their present form.

Previously, Grady and Hollenbach (1979), Grady and Kipp (1981), and

Cohn and Ahrens (1981) obtained dynamic tensile strength data on igneous rocks and oil shale. In the present study we have carried out several cratering experiments in a well-characterized gabbro in the 10^9 to 10^{10} erg energy range, and performed measurements of the dynamic tensile strength in the same material at strain rates of 10^5 to 10^6 sec^{-1}. We have applied the dynamic fracture data to the cratering results by employing Melosh's (1983) theory, as well as describing the distribution of compressive and shear failure fragments using the formulation of Grady and Kipp (1980).

2. Sample, San Marcos gabbro

San Marcos gabbro (Escondido, California) is a basic intrusive igneous rock (Table I, Figure 1). The present samples contain relatively large plagioclase grains (1 to 3 mm) and amphibole (1 to 2 mm) intergrown with pyroxene and biotite (Larsen, 1948; Miller, 1937). On a microscopic level, the sample is essentially crack-free with cracks and fractures of less than 1 mm being absent. However, incipient microcracks are present along grain boundaries. The density of sample material used was 2.867 g/cm^3 and the compressional wave velocity, C_p=6.36± 0.16 km/sec, was determined at 10 Mhz.

3. Cratering Experiments

a) Experimental Details

Cubic blocks, ~ 20 cm on a side, were cut from samples and a polished surface was impacted. The target blocks were embedded in cylindrical concrete blocks approximately 30 cm in diameter and 30 cm height. Inverted aluminum cans, 30 cm in diameter, and lined with styrofoam, were suspended about 20 cm above the top surface of the gabbro in order to catch high speed ejecta. The target assembly was then inserted in the target chamber of the NASA Ames Vertical Gun Facility. Prior to each experiment, the chamber was evacuated and the target was impacted with spherical, pyrex glass stainless steel and lead projectiles 3.2 mm in diameter (Table II).

b) Results

Figure 2a,b,c illustrates the effect of impact of a lead projectile (Shot 3). The resulting crater is highly irregular in outline and its morphology is characterized by relatively large flat spall surfaces. Clearly visible are radial cracks which also reflect the shape of a larger recovered ejecta fragments (Figure 2b). The fragments also show incipient cracks which follow a concentric pattern. Reflecting the irregular crater shape, the ejecta fragments differ in size and shape; however all the spall fragments are plate-like and are easily fit back into the crater (Figure 2c). Some 60 to 80% of the crater volume is taken up by these large spall fragments which remained intact whereas the remaining volume of the crater consisted of completely fragmented small fragments in the 2 to 3 cm to submillimeter size range. The impact of the stainless steel projectile (Shot 1) resulted in a similar crater and ejecta fragment characteristics. In Figure 3, the cross-section through a crater (Shot 2) shows the relatively large flat shallow spall surfaces and the generally rough and irregular outline of the crater. Also visible is the central trough which is observed in all targets. This trough is similar to that observed by Moore et al. (1963) and Hörz (1969) in which the central portion of the rock fails in compression and shear and is excavated when the resulting small fragments are ejected. Based on the distribution and shape of ejecta fragments we conclude that whereas the trough contained highly fragmented small ejecta, the upper large portion of the crater contained relatively few large fragments.

The variance from simple energy scaling can be seen in the crater

dimensions given in Table II. Although the energy of the pyrex impactor is comparable to that of the lead and stainless steel impactors the resulting crater was considerably smaller. However, even taking this into account the present crater volumes are a factor of 3 larger than those obtained in a variety of rocks by Moore et al. (1963) and in granodiorite by Hörz (1969).

All ejecta fragments for Shots 1 and 3 were collected and the fragment size and fragment shape distribution, the latter only for large fragments, are shown in Figures 4 and 5. We plot the fragment mass, m, of the larger ejecta fragments (mass > 0.1 g), versus, cumulative number of fragments, N_f, according to

$$\log_{10}(N_f) = a + b \log_{10}(m) \qquad (1)$$

The slope, b, of the lines fit to these data provides a measure of the degree of fragmentation of the target. Smaller values of b indicate distributions which are dominated by smaller fragments whereas in the present case the distributions with predominantly large fragments result in larger values of b. The slopes for our distribution lie at about -0.5 to -0.6, a value generally in agreement or slightly higher than those reported in the literature. Hartmann (1969) obtained b values which varied from -0.6 to -1.2. Fujiwara et al. (1977) found b values of -0.4 to -0.7 for impacts into basalt whereas Lange and Ahrens (1981) obtained values ranging from -1.0 to -1.8 for impacts into ice and ice silicates.

We measured the long (A), intermediate (B), and short (C) axes for

all the larger fragments from Shots 1 and 3. Figure 5 shows the observed ratios, B/A, versus, C/A which allow characterization of fragment shape (Lange and Ahrens, 1981). Values of B/A and C/A approaching unity and zero respectively are for ideal plate-like fragments. As is evident from the figure, most of the fragments have B/A values greater than 0.6 and C/A values less than 0.25 with means of 0.77 ± 0.13 and 0.73 ± 0.11, and 0.21 ± 0.07 and 0.16 ± 0.06 for Shots 1 and 3, respectively. The above values indicate that the larger ejecta fragments are plate-like and presumably are spall fragments. The smaller fragments (< 0.2 g) from Shots 1 and 3 were sieve-analyzed to obtain a fragment size distribution in order to determine a principal fragment dimension (Figure 6). The fragment size distribution for both shots were similar and demonstrate that most of the fragments are less than 0.1 to 0.12 mm in size.

In summary, the present impact experiments on San Marcos gabbro resulted in craters which are characterized by spallation of a few large plate-like fragments. Both the fragment mass distribution and the fragment shape distributions lead to this conclusion. Completely fragmented shear and compression failured material is probably derived from the central section of the crater and is dominated by fragment sizes of less than 0.1 to 0.12 mm size. The principal crater forming processes is tensile failure (spallation), which, as discussed in Section 6, results from release wave interaction near the impacted surface of each target block. Thus, classification of these experiments and derivation of possible scaling laws requires knowledge of the dynamic tensile strength of the rock on an appropriate time scale.

4. Dynamic tensile strength measurements

a) Experimental details

The dynamic tensile strength of San Marcos gabbro was determined using techniques similar to those of Cohn and Ahrens (1981). The impact of a plexiglas flyer plate onto a cylindrical sample (20 mm diameter, 6 mm thick) generates compressional waves which upon reflection from the free surfaces of a flyer and sample become rarefaction waves. Appropriate dimensions of the flyer and sample allow interaction of these two rarefaction waves and a state of tensile stress in one-dimensional strain to be obtained in the middle of a sample. Varying impact velocities result in different amplitude tensile stresses. Upon sample recovery the stress levels required to produce incipient and complete tensile failure of samples may be determined (Lange and Ahrens, 1982). The experimental parameters of the experiments (Table 3) are such that the strain rates varied from between 10^4 to 10^5 sec^{-1} which is comparable to the strain rates associated with the impact experiments of the previous section. The impacted samples were recovered intact. Radial cross-sections were polished and thin sections were examined under an optical microscope to obtain crack statistics.

b) Results

The length and condition of small cracks observed in thin sections of the shock loaded samples is given in Table III. Figure 7 gives

examples of observed cracks and explains the terminology used to describe the cracks. In samples which experienced only low or moderate tensile stresses, cracks propagated only along the grain boundaries. With increasing stress level an increasing number of cracks were observed to propagate through grains, generally following a direction parallel or subparallel to the impacted surface of the sample. Several cases of coalescence of cracks which started out either parallel to each other from one side of the sample or which met within the sample but originated in opposite directions were observed. Branching of cracks was not observed. In most of the samples cracks were closed and only samples from the highest stress levels (above 170 Mpa) had open cracks. In order to identify those cracks which cause tensile failure, the following criteria were employed: (1) We identified only cracks greater than 0.5 mm long. (2) Only cracks running parallel or near-parallel to the impact surfaces were counted, and (3) Only cracks close to the mid-plane of each sample; i.e., the region of maximum tensile stress, were counted. Figure 8 shows the number of cracks selected according to the above criteria as a function of tensile stress from all samples. As can be seen, for peak tensile stress of ~ 150 Mpa the onset of large continuous spall cracks (greater than 1-2 mm long) was taken to indicate stresses in excess of the dynamic tensile strength. The mean value of tensile stress for these samples was 147 $\pm$ 9 Mpa. This result agrees with earlier results for an anorthositic gabbro but is distinctly greater than the values of 70 to 110 Mpa measured for quartzose rocks (Cohn and Ahrens, 1981).

5. Continuum Fracture Model for Gabbro

In order to extrapolate the present results for dynamic tensile strength to other strain rates, we attempt to generalize our findings in terms of the continuum fracturing model of Grady and Kipp (1980). We estimated the value of the principal fragment size, L_m, for the totally fragmented target portion of our sample, the time, T_m, at which maximum stress is reached in the sample, and the time, T_f, at which tensile failure conditions are satisfied (Table 4). In the Grady-Kipp model, the values of k and m are the two parameters of the Weibull crack distribution and

$$n = k\varepsilon^m \tag{2}$$

where n is the number of flaws per volume which can be activated at or below tensile strain level, ε. The values of k and m which relate principal fragment size to strain rate and tensile strength are:

$$L_m = 6\, C_g/(m+2)\, \alpha^{-1/(m+3)}\, \dot{\varepsilon}^{-[m/(m+3)]} \tag{3}$$

and

$$\sigma_m = K(m+3)(m+4)^{-(m+4)/(m+3)}\alpha^{-1/(m+3)}\dot{\varepsilon}^{3/(m+3)} \tag{4}$$

where

$$\alpha = \frac{8\pi C g^3 k}{(m+1)(m+2)(m+3)} \tag{5}$$

Here, $K \cong 5/9\ C_p{}^2\rho$, the elastic modulus for one-dimensional strain where C_p is the p-wave velocity and ρ the density of the sample. Also, C_g is the growth velocity for activated cracks. The model of Table IV provides theoretical values of α_m, L_m, t_m, and t_f. The values of $m=9.1$, and $k=10^{46}$, are comparable to those found for ice and ice-silicate mixtures (Lange and Ahrens, 1982) and lie above values of m and k obtained by Grady and Kipp for oil shale. The value of $C_g=2.56$ km/sec, lies at the upper end of the plausible range of C_g:

$$C_p/3 < C_g < 2/5\ C_p \tag{6}$$

The values of k and m are used to predict variation of tensile strength as a function of strain rate in Figure 9.

6. Crater Spall Fractures

Comparisons of cratering efficiencies observed in the present experiments (Figure 10) with those observed for a variety of decimeter-sized craters in various rocks by Moore et al. and Hörz (1969) demonstrate that the present largely spall crater volumes are larger by a factor of 2 to 3 than those of previous cratering studies. In metals, the cratering efficiency can be described in terms of:

$$\pi_1 = V\rho/M \tag{7}$$

where V, ρ, and M are the volume of the crater, the density of the

target, and the mass of projectile, respectively (Holsapple and Schmitt, 1982). For a series of impacts of metals onto metal, the density scaling parameter

$$\pi_3 = \delta/\rho \tag{8}$$

and strength parameter

$$\pi_4 = Y/\delta U^2 \tag{9}$$

were fit to the relation for different impacts given by

$$\pi_1 \left[\pi_3^{0.738}\pi_4\right]^{0.709\pm0.027} = 0.48\pm0.080 \tag{10}$$

Here, δ and U are projectile density and velocity and Y is effective material strength. Upon applying Equations 9 and 10 to calculate for the craters produced by polyethylene impacts into Vacaville basalt (Moore et al., 1963), impact of aluminum onto granodiorite (Hörz, 1969) and the present experiments, yield values of Y in the range of 3-6 Mpa. These values on the order of 10^{-4} times the elastic moduli of these competent rocks. We infer that rather than yielding the effective shear or compressive failure strength the assumption underlying the strength scaling (Equations 9 and 10) does not really apply. As already pointed out in the present cratering experiments, most of the crater volume is the result of spall failure. The present measurements of spall strength of gabbro (~147 Mpa) suggests that this is high, relative to that of

quartzose rocks (Figure 9). Recent measurements of the fracture energy of olivine (Swain and Atkinson, 1978) indicate that its surface energy is comparable to that of quartz (~1 J/m^2). Moreover microcline has an even greater surface energy (~3-5 J/m^2) (Atkinson and Avdis, 1980). No simple reason can now be given for the greater spall strength of gabbro and basalt than those of quartz-bearing rocks. Hence, there is no straightforward correlation between spall strength or spallation of a certain material and its value for the surface energy. As was noted earlier (Grady and Kipp, 1980), the amount of energy needed to create the combined surface area of all fragments in a fragmentation experiment does not agree with the energy imparted in the target body due to the impact.

Taking the dynamic tensile strength of 147 Mpa, the theoretical maximum spall thickness, z_s, can be calculated from a wave interaction treatment of Melosh, 1983. Using his hydrodynamic approximation of spall thickness as a function of radius, r, which is given as

$$z_s = \frac{\sigma_t \, r^{(n+1)}}{C_p \, \delta U a^n \, [1-nd/r]} \tag{11}$$

where a is the equivalent projectile diameter and d is the assumed explosive equivalent depth of impact. Here d is assumed to be given as

$$d \simeq 2a \, (\delta/\rho)^{1/2} \tag{12}$$

The elastic shock pressure p is assumed to decay according to the

approximation

$$P = \rho C_p U(a/r)^n/2 \qquad (13)$$

where n is 1.87. The value of n chosen by Melosh is close to the value found for the decay of peak pressure from impacts in the 7.5 to 15 km/sec range by Ahrens and O'Keefe, 1977. Notably the spall surfaces predicted by Eq. 11 are convex upward which is opposite to what is observed (Figure 10). Using the measured values of the parameters in Equation 11 yields predicted spall thicknesses of ~1.5 cm (Figure 11). These values are comparable to the maximum value observed. The average spall thicknesses is ~1 cm at a diameter of 4 cm for the two experiments for which intact spalls were recovered (Figure 11). An interesting prediction of Equation 11 are thinner spalls for weaker tensile strength materials. The available data for spall strength (Figure 9) and the resulting cratering efficiency (Figure 12) agree at least qualitatively with this prediction.

7. Conclusions

Application of the Grady-Kipp (1980) fracturing model to the present data for fragment size and dynamic tensile strength yields a prediction dependence of tensile strength on strain rate. Hypervelocity impact experiments producing deci-centimeter sized craters in gabbro yield crater morphologies which appear to be dominated by spalling or tensile fracture. Melosh's (1983) theory of near-surface spalling is

used to predict a value of maximum spall thickness of 1.5 cm which compares favorably with observed spall thicknesses of ~1 cm observed in the present experiments. The enhanced cratering efficiency due to spalling is such that the cratering efficiency is increased from the 2 to 3 x 10^{-9} g/erg for siliceous rocks to 6 x 10^{-9} g/erg for the present basic, high-tensile strength rocks. This effect of spallation-induced cratering appears, in at least the present experiments, to enhance the proposed (Melosh, 1983) impact-induced projection of ejecta from lightly shocked surface material from the surfaces of moon and Mars.

Acknowledgments

We thank R. Weldon for collaboration in carrying out the impact experiments at NASA Ames Vertical Gun Facility. We appreciate the planning and execution of the tensile strength experiments of S. N. Cohn and R. Manning and the technical assistance of E. Gelle and M. Long. M. Lange was supported by a stipend from the Deutsche Forschungsgemeinschaft. Work supported by NASA Grant NGL-05-002-105 and NASA Grant NSG 7129. Contribution No. 3943, Division of Geological and Planetary Sciences, California Institute of Technology.

References

Ahrens, T. J. and O'Keefe, J. (1977). Equation of state and impact-induced shock wave attenuation. In Impact and Explosion Cratering, Roddy, D. J., R. O. Pepin, and R. B. Merrill, eds., Pergamon Press, 639-656.

Atkinson, B. K. and Avdis, V. (1980). Fracture mechanism parameters of some rock-forming minerals determined using an indentation technique, Int. J. Rock Mech. Min Sci. & Geomech. Abstr., 17, 383-386.

Cohn S. N. and Ahrens T. J. (1981). Dynamic tensile strength of lunar rock types, J. Geophys. Res., 86, 1794-1802.

Curran, D. R., Shockey, D. A., Seamen, L. and Austin, M. (1977). Mechanisms and models of cratering in earth media, in Impact and Explosion Cratering, Roddy et al., eds., Pergamon Press, New York, pp. 1057-1087.

Fujiwara, A., Kamimoto, G., and Isukamoto, A. (1977). Destruction of basaltic bodies by high velocity impact, Icarus, 31, 277-288.

Grady, D. E. and Hollenbach, R. E. (1979). Dynamic fracture strength of rocks, Geophys. Res. Lett., 6, 73-76.

Grady, D. E. and Kipp, M. E. (1980). Continuum modelling of explosive fracture in oil shale, Int. J. Rock Mech. Min Sci. & Geomech. Abstr., 17, 147-157.

Hartmann, W. K. (1969). Terrestrial, lunar, and interplanetary rock fragmentation, Icarus, 10, 201-213.

Holsapple, K. A. and Schmitt, R. M. (1982). On scaling of crater

dimensions 2. Impact processes, J. Geophys. Res., 87, 1849-1870.

Hörz, F. (1964). Structural and mineralogical evaluation of an experimentally produced crater in granite, Contrib. Min. Petrol., 21, 265-277.

Lange, M. A. and Ahrens, T. J. (1981). Fragmentation of ice by low velocity impacts, in Proc. Lunar Planet. Sci. Conf. 12th, Pergamon Press, New York, pp. 1667-1687.

Lange, M. A. and Ahrens, T. J. (1982). The dynamic tensile strength of ice and ice-silicate mixtures, J. Geophys. Res., 88, 1197-1208.

Larsen, E. S., Jr. (1948). Batholith and associated rocks of Corona, Elsinore, and San Luis Rey quadrangles, Southern California Geol. Soc. America, Mem. 29, 182 pp.

Melosh, H. J. (1983). Impact ejection, spallation and the origin of meteorites, submitted to Icarus.

Miller, F. S. (1937). Petrology of the San Marcos gabbro, Southern California, Bull. Geol. Soc. Amer., 48, 1397-1426.

Moore, H. J., Gault, D. E., and Lugn, R. V. (1963). Experimental impact craters in basalt, Trans. Soc. Mining Engineers, 229, 258-262.

Shockey, D. A., Curran, D. R., Seaman, L. Rosenberg, J. T., and Petersen, C. F. (1974). Fragmentation of rock under dynamic load, Int. J. Rock Mech. Sci. & Geomech. Abstr., 11, 303-317.

Stolper, E., McSween, H. Y., Jr., Hays, J. F. (1979). A petrogenetic model of the relationships among achondritic meteorites, Geochim.

Cosmochim. Acta, 43, 589-602.

Swain, M. V. and Atkinson, B. K. (1978). Fracture surface energy of olivine, Geotis. pura. appl., 116, 866-872.

Wasson, J. T. and Wetherill, G. W. (1979). Dynamical, chemical and isotopic evidence regarding the formation location of asteroids and meteorites, in Asteroids, T. Gehrels, ed., U. Ariz. Press, pp. 926-974.

Wood, C. A. and Ashwal, L. D. (1981). SNC meteorites: Igneous rocks from Mars?, Proc. Lunar Planet. Sci. 12B, 1359-1375.

Figure Captions

Figure 1. Photo-micrograph of pristine San Marcos gabbro. The light mineral grains are predominantly plagioclase and amphibole. The dark grains are pyroxene and biotite.

Figure 2. Experimental impact crater in San Marcos gabbro resulting from impact of a lead projectile (mass = 0.2g, impact velocity, 4.6 km/sec). (a) crater, (b) recovered large fragments, (c) reconstructed spall fragments.

Figure 3. Photo-micrograph cross-section of experimental crater in San Marcos gabbro. Impact of a pyrex sphere (mass = 0.04g, impact velocity = 6.3 km/sec).

Figure 4. Mass distribution (> 0.1g) of fragments from cratering Experiments 1 and 3 in San Marcos gabbro. Parameters fit to Eq. 1 for Shot #1 are a = 1.02 and b = -0.57 and for Shot #3 are a = 0.97 and b = -0.48.

Figure 5. Fragment shape distribution for fragments (masses > 0.1g) of cratering Experiments 1 and 3 in San Marcos gabbro. A is the long, B the intermediate, and C the short axis of each fragment, respectively.

Figure 6. Size distribution of smaller fraction (masses < 0.1g) of fragments from cratering experiments 1 and 3 in San Marcos gabbro obtained in sieve analysis.

Figure 7. Photo-micrographs of shock loaded San Marcos gabbro. Distribution and morphology of spall cracks resulting from tensile failure at strain rates of $\sim 10^4$ to 10^5 sec^{-1}.

Numbers represent tensile stress. Scale bar corresponds to 1 mm.

Figure 8. Number of spall cracks as a function of peak tensile stress observed on thin sections of shock loaded San Marcos gabbro. Occurrence of continuous, larger cracks (> 0.5 mm), in the mid-plane of each thin-section marks stresses equal to, or, exceeding the dynamic tensile strength of sample.

Figure 9. Tensile strength as a function of strain rate for San Marcos gabbro and other geological materials. Dashed line represents a theoretical prediction.

Figure 10. Spall fragments from Shot #3. Shown is the bottom of the large spall fragments demonstrating that spall surfaces are oriented opposite to what is predicted by theory.

Figure 11. Cross-sections of spall fractures produced in Shot #3 and theoretical spall surface calculated from Eq. 11.

Figure 12. Relation of projectile energy to experimental crater volumes for various rocks.

Table I. Mineralogical composition of San Marcos gabbro sample

Mineral	Volume %
Plagioclase	67.9
Amphibole	22.5
Clinopyroxene	1.5
Orthopyroxene	1.1
Quartz	1.4
Biotite	0.9
Opaques	4.3
Alkali feldspar	trace
Calcite	trace
Chlorite	trace
Apatite	trace
	Σ = 99.6%

(Analysis by Robert Hill)

Table II. Experimental parameters and results of cratering experiments on San Marcos gabbro

Shot No.	Target Material	Target Mass, g	Projectile			Crater		
			Mass, g	Velocity, km/sec	Impact Energy, 10^{10} ergs	Diameter,(1) mm	Depth,(2) mm	Volume,(3) cm^3
1	Stainless Steel	20270	0.143	5.2	1.9	118	13	40.5
2	Pyrex	--(4)	0.044	6.3	0.87	24(4)	5(4)	--(4)
3	Lead	18300	0.195	4.6	2.1	113	13	43.8

(1) Mean value of four measurements.

(2) Mean value of three measurements.

(3) Derived from mass of fine grained sand (mean grain size ~0.1 mm, mean density 1.44 g/cm^3) used to fill crater volume.

(4) Only measurements on two thin sections, cut diametrically through crater were carried out.

Table III. Experimental parameters for tensile strength experiments on San Marcos gabbro, Results of microscopic analysis.

Imp. vel. m/s	Peak Stress MPa	Sample No.	Description of Cracks: Crack Type	Crack Lengths, mm <0.5	0.5-1	1-2	2-4	>4	Comments
28.3	80.5	SMG 1	No visible cracks						
31.1	88.4	SMG 8	No visible cracks						
34.4	97.8	SMG 2	Incipient, not well-developed	1	2				
37.8	107.5	SMG 7	No visible cracks						
47.2	134.2	SMG 10	No visible cracks						
47.3	134.5	SMG 6	Incipient, partially developed cracks		3	1			
51.0	145.0	SMG 22	Several incipient cracks, system of continuous, fairly well-developed cracks	4		4	2		
53.7	152.7	SMG 23	Several incipient cracks, few fairly well-developed shorter cracks, more or less continuous well-developed cracks		3	2	2		
54.1	153.8	SMG 3	Incipient crack, continuous, well-developed system of cracks		1		1	1	
58.2	165.5	SMG 9	Incipient cracks, poorly developed crack		1	1			
59.8	170.0	SMG 24	Incipient cracks, fairly well-developed systems of cracks, continuous, relatively long, spall cracks	1		4	2	2	

Table III. Continued

Imp. vel. m/s	Peak Stress MPa	Sample No.	Description of Cracks: Crack Type	Crack Lengths, mm <0.5	0.5-1	1-2	2-4	>4	Comments
60.0	170.6	SMG 26	Incipient cracks; fairly well-developed systems of cracks, less well-developed continuous cracks			3	2	1	
62.1	176.6	SMG 4	Incipient crack, well-developed continuous cracks		4		1	1	
67.1	190.8	SMG 25	Incipient cracks; fairly well-developed cracks; long, continuous cracks (crack system)			1	1	2	Longest crack observed (10.5 mm)
70.1	199.3	SMG 21	Incipient cracks; well-developed cracks (crack system), system of continuous cracks	3	1	3	2	4	
71.9	204.4	SMG 11	Incipient cracks, well-developed spall cracks; systems of relatively long cracks		3	4	4	3	Best developed cracks; clear spall cracks. Stress >> spall strength
77.5	220.3	SMG 5	Incipient cracks; system of continuous cracks			2	2		
80.8	229.7	SMG 12	Incipient cracks; well-developed spall cracks; system of continuous cracks		1	3	5		

Table IV. Continuum fracturing model parameters for San Marcos gabbro and comparison with numerical results

$\dot{\varepsilon}$ (sec^{-1})	m	k	C_g (km/sec)	σ_m (MPa)		L_m (mm)		t_m (μsec)		t_f (μsec)	
				observed	theoretical	observed	theoretical	observed	theoretical	observed	theoretical
1	9.1	10^{46}	2.56(1)	$10^{(2)}$	10.1	--	2.9×10^{2}	--	1.7×10^{2}	--	2.1×10^{2}
5×10^{4}	9.1	10^{46}	2.56(1)	147± 9	147.2	0.1-0.12(3)	0.1	$\lesssim$ 0.9(4)	0.5	$\lesssim$ 0.9(4)	0.6

(1) $C_g \simeq 0.4\ C_p$

(2) Derived from strength values for Westerly granite in "static" tests (Grady and Hollenbach, 1973).

(3) L_m was obtained from a sieve-analysis of completely fractured target material in cratering experiments on San Marcos gabbro.

(4) Derived for total duration of tensile strain pulse in the samples; i.e., t_m and t_f have to be smaller than this time.

TJA83140SPH

Fig. 1

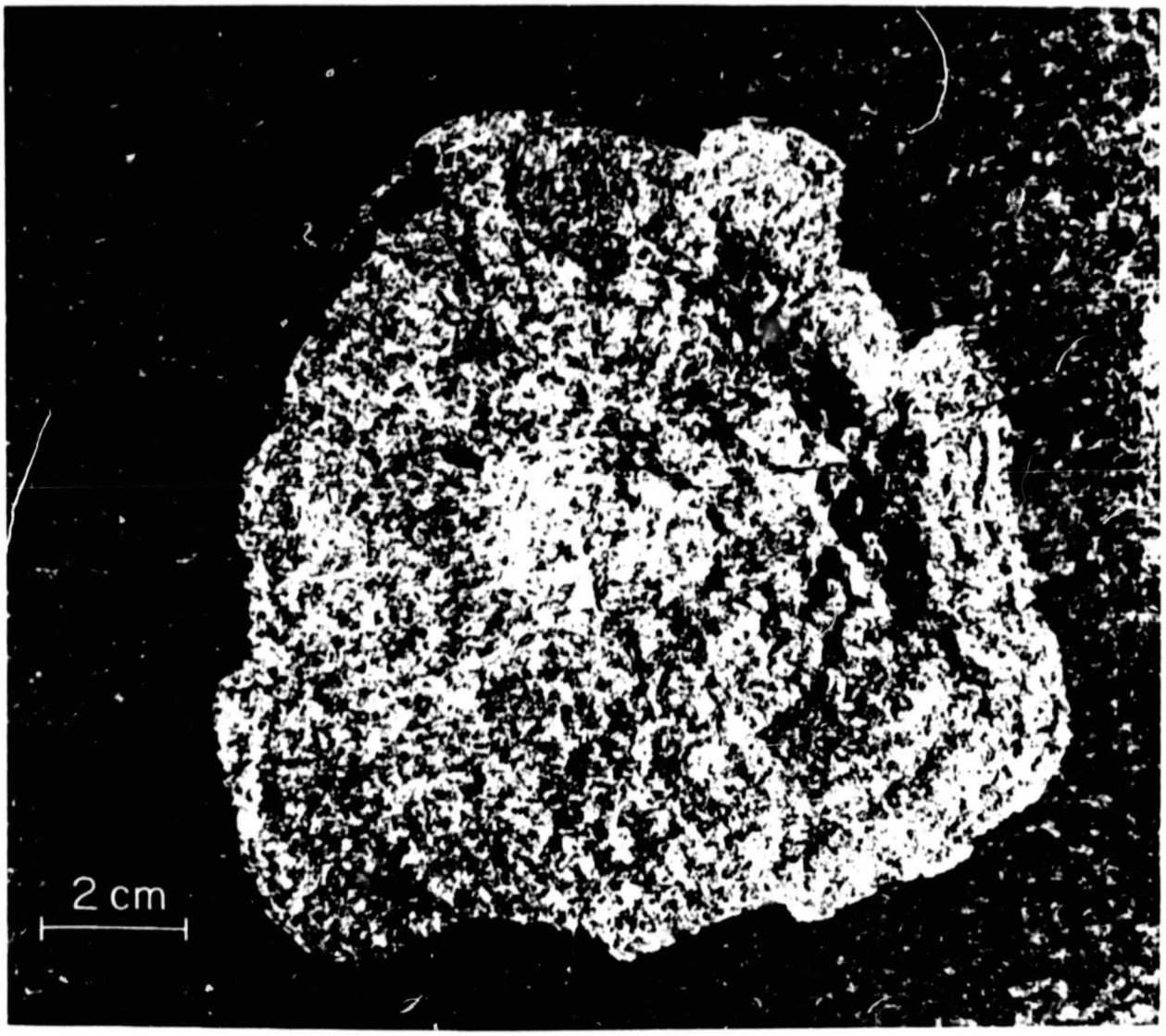

TJA83141SPH

Fig. 2a

ORIGINAL PAGE IS
OF POOR QUALITY

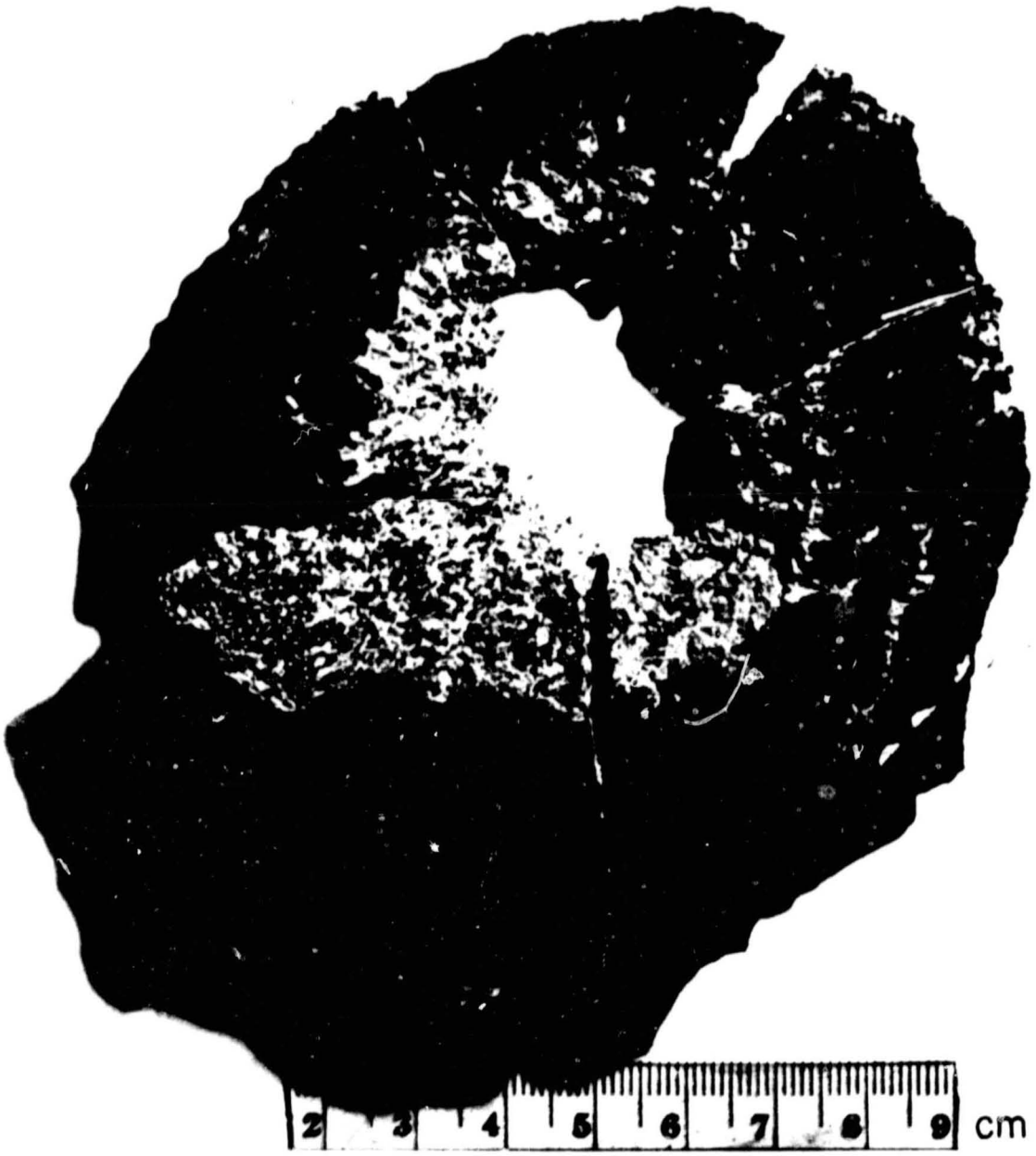

TJA83142SPH

Fig. 2b

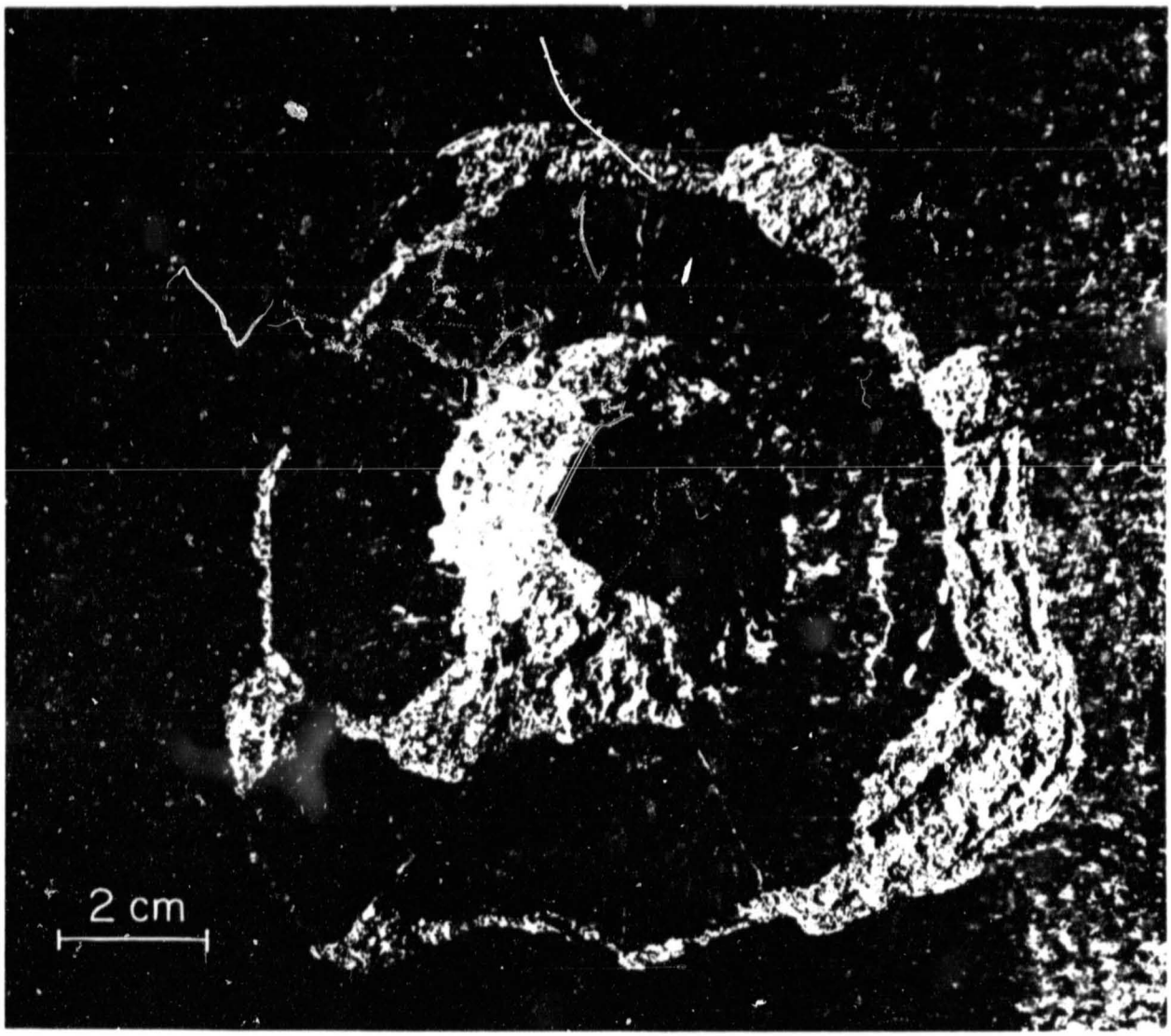

TJA83143SPH

Fig. 2c

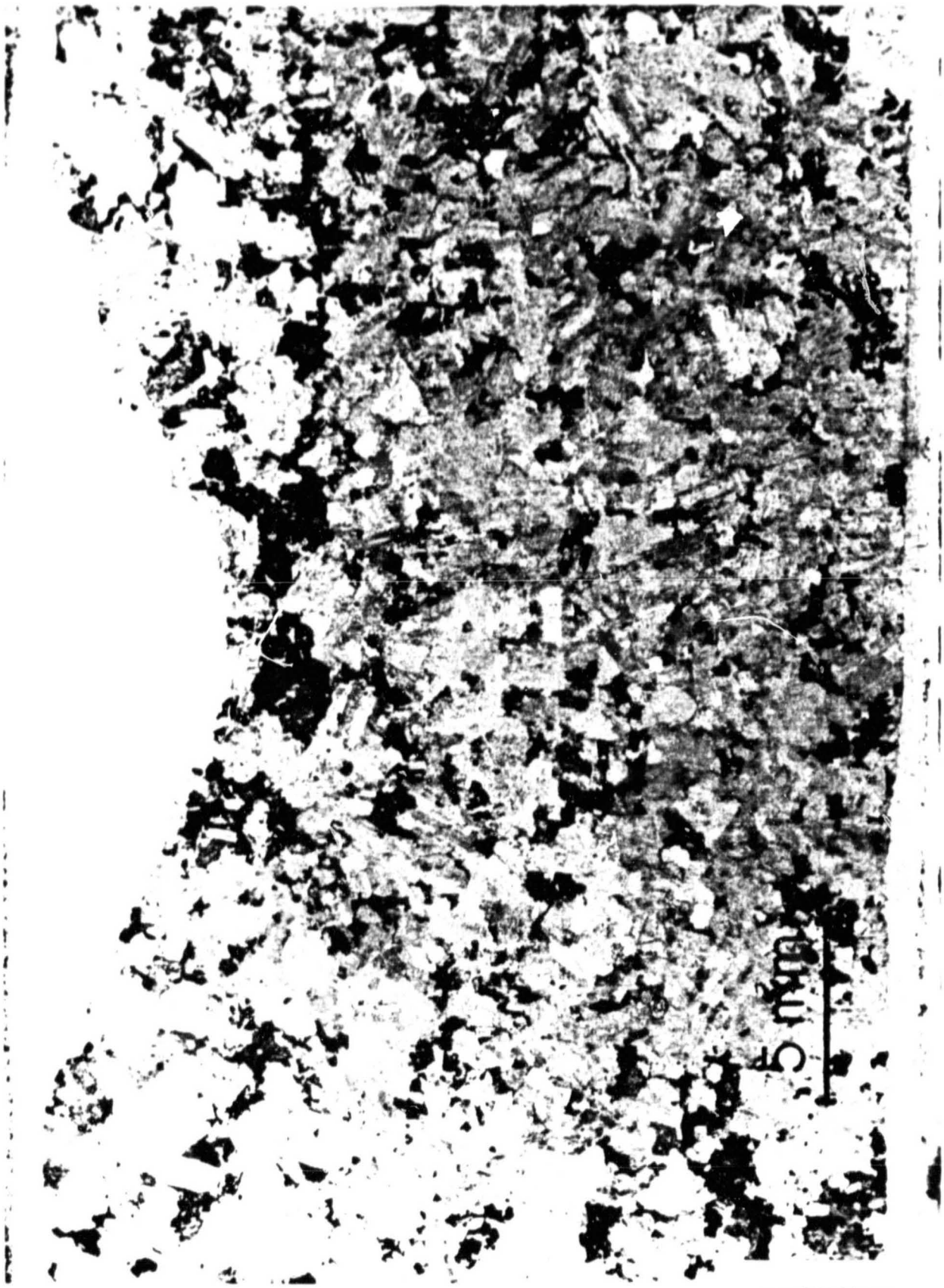

TJA83144SPH

Fig. 3

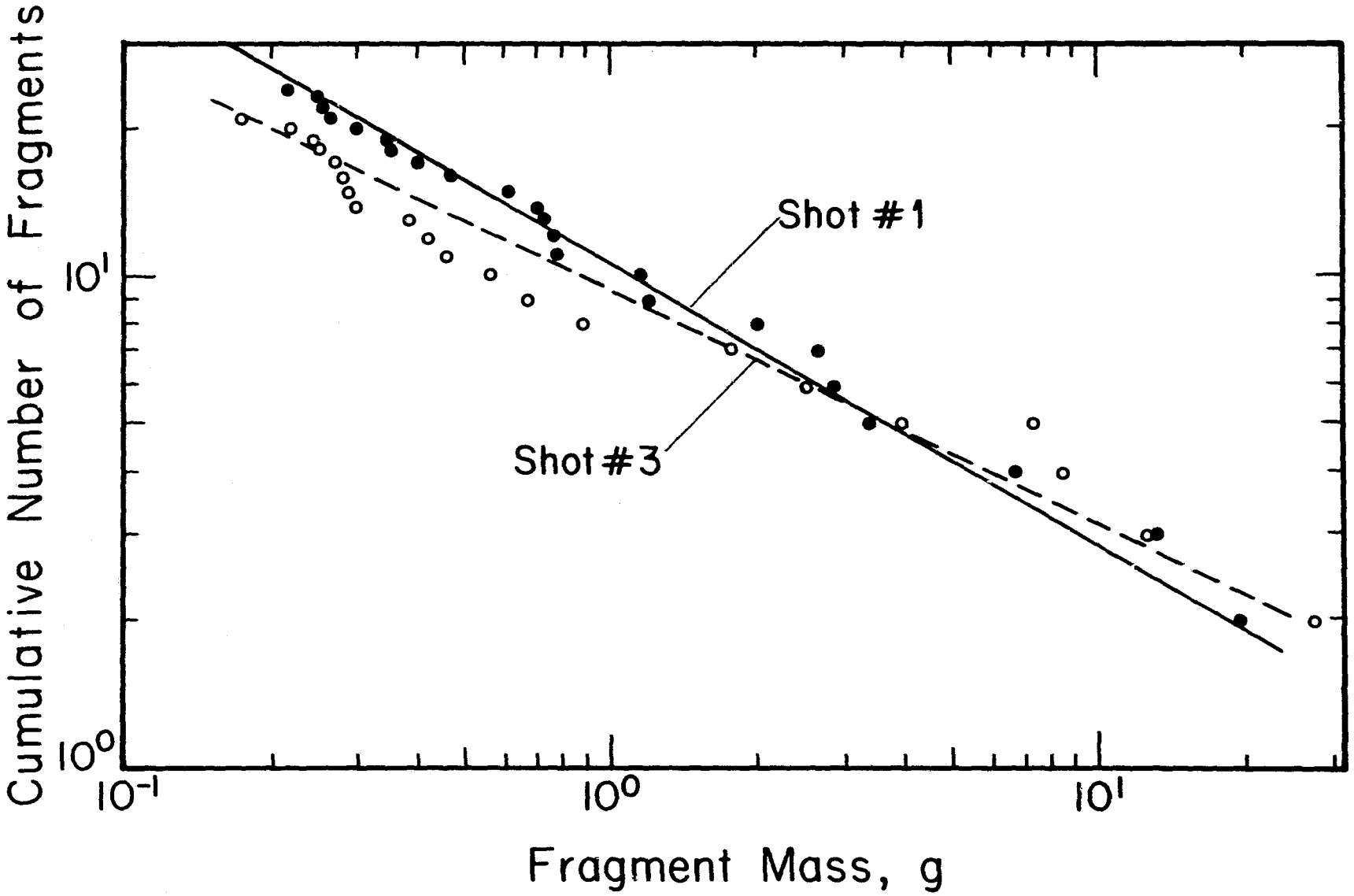

Fig. 4

TJA83145SFD

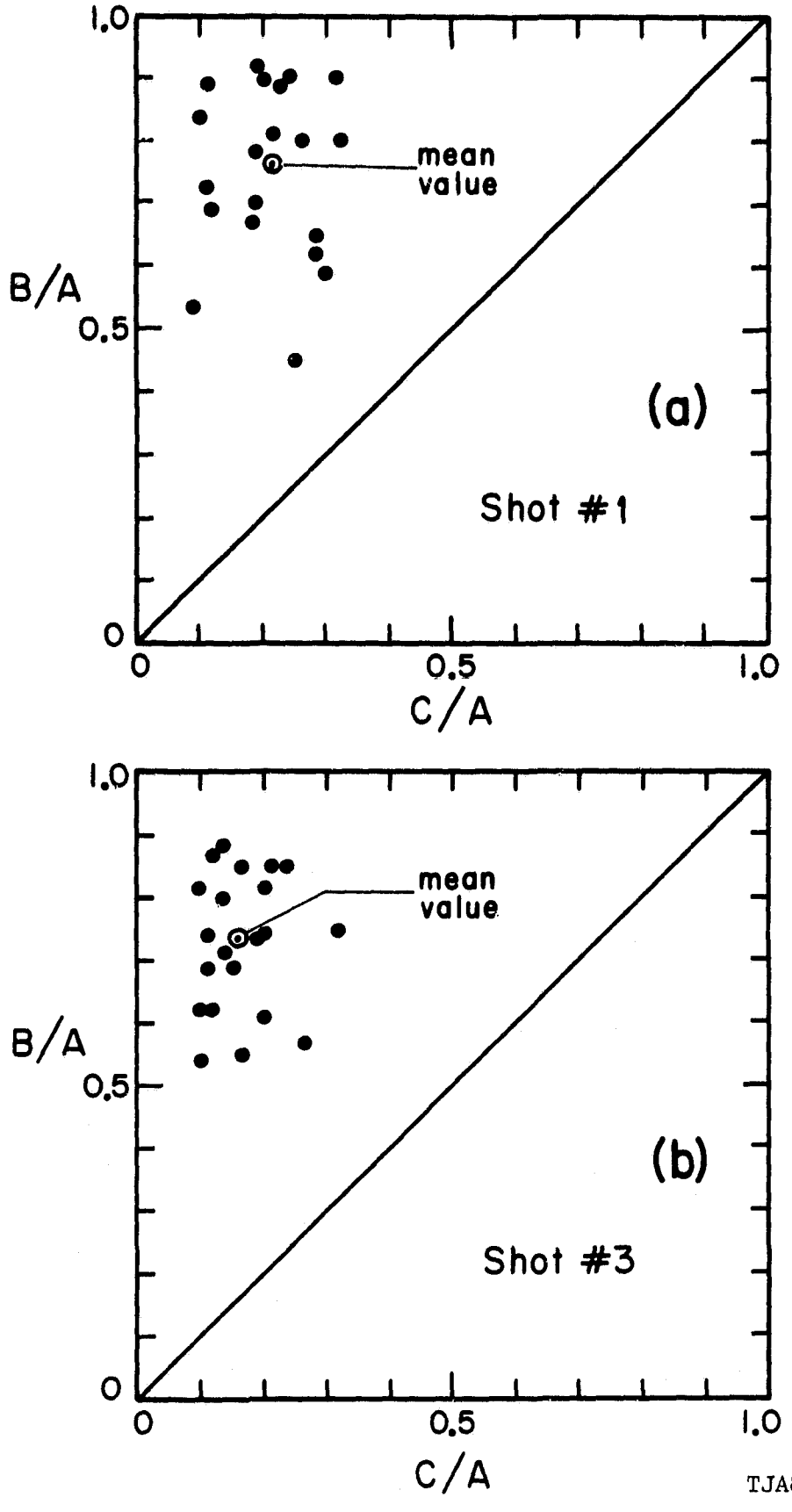

TJA83146SFD

Fig. 5

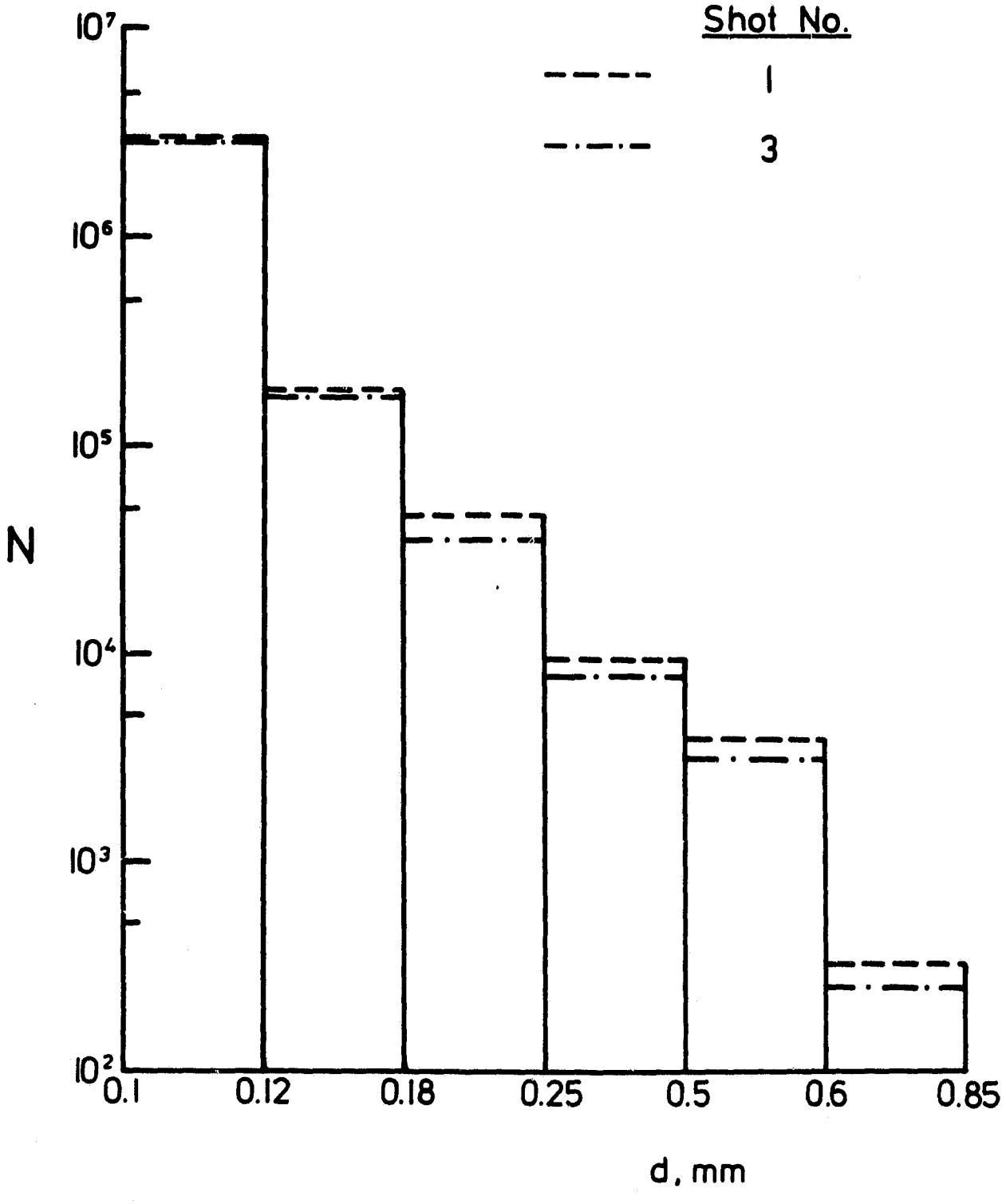

TJA83147SFD

Fig. 6

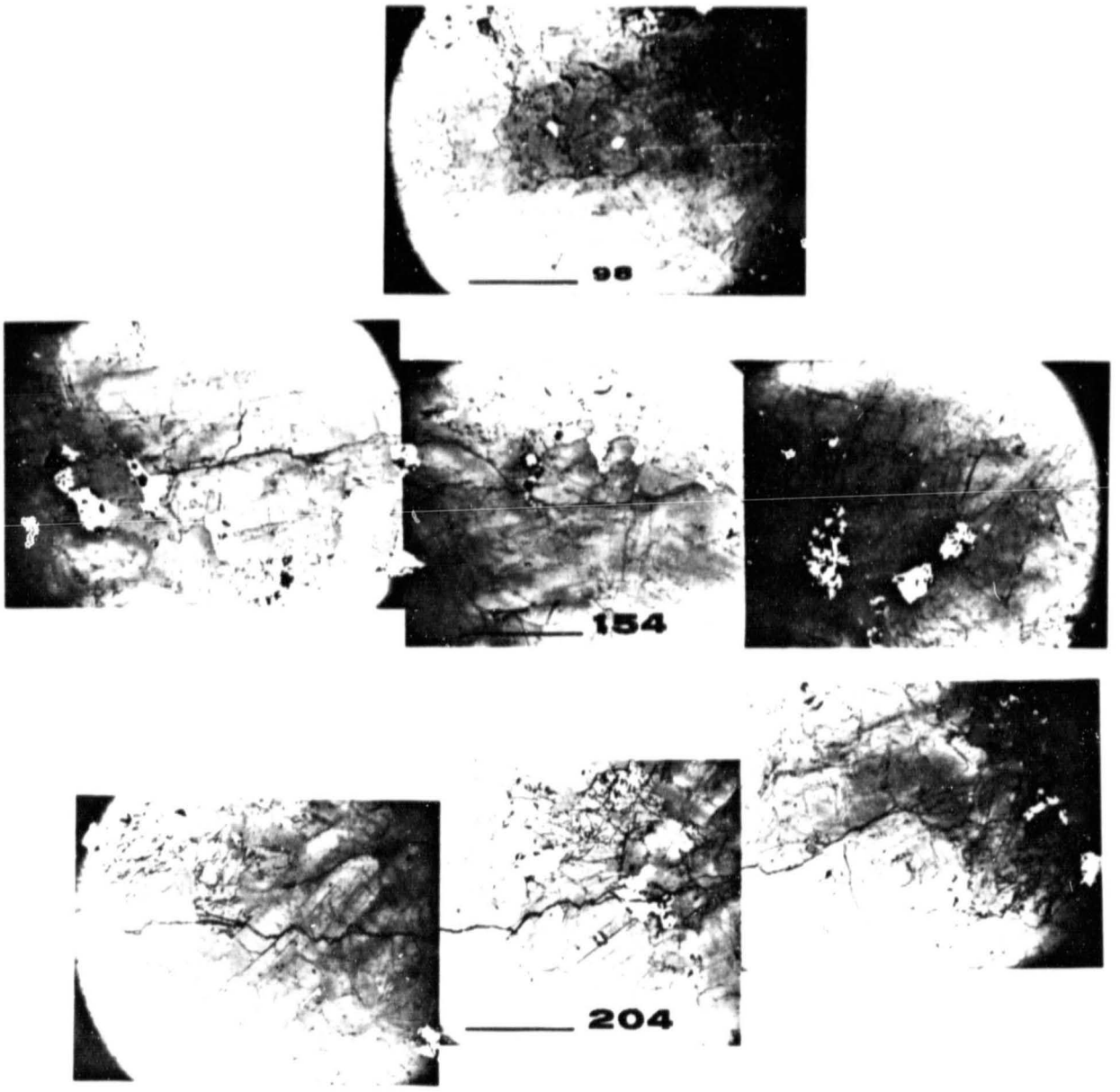

Fig. 7

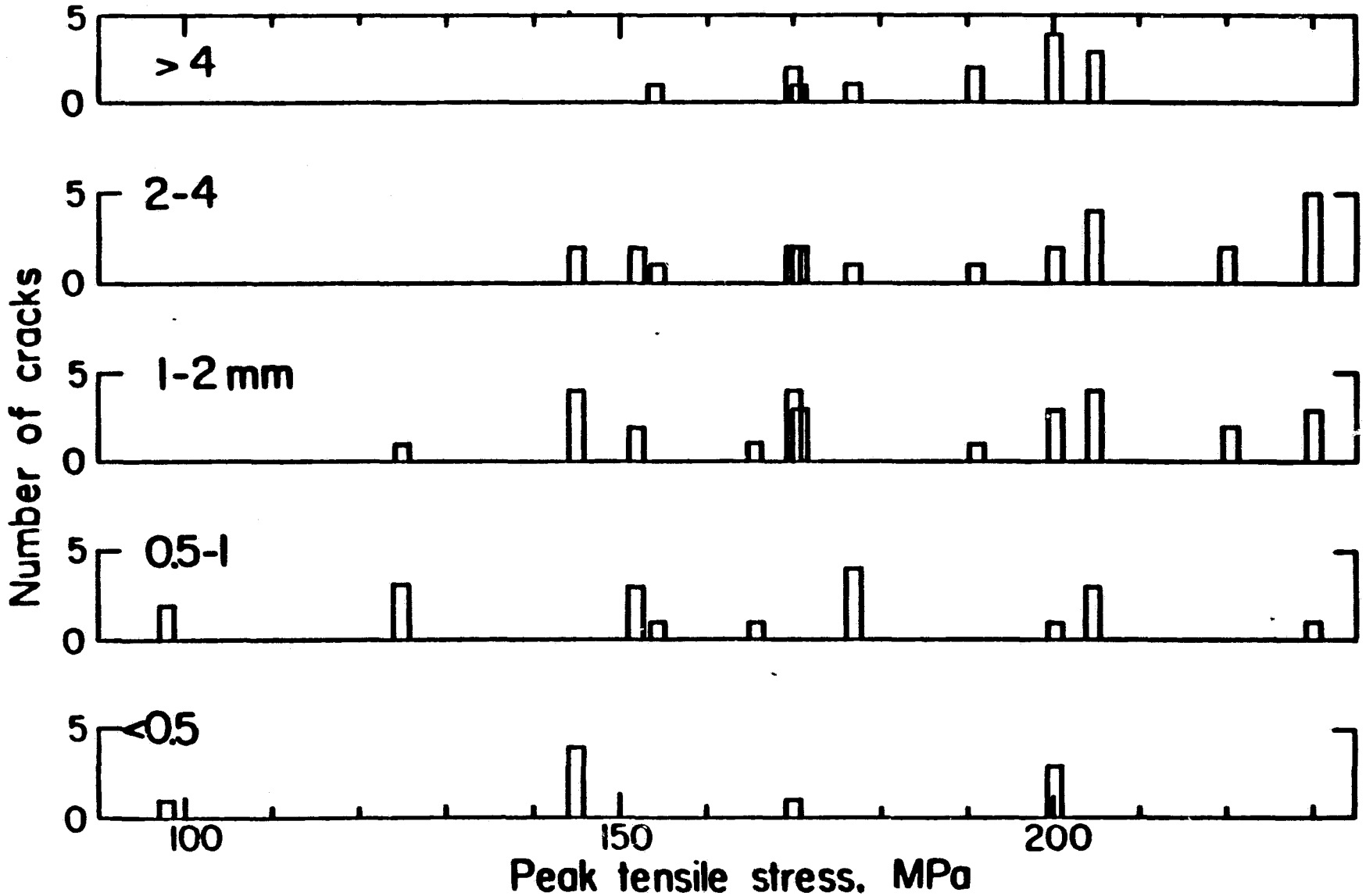
>4
2-4
1-2 mm
0.5-1
<0.5
5
0
Number of cracks
100
150
200
Peak tensile stress, MPa

Fig. 8

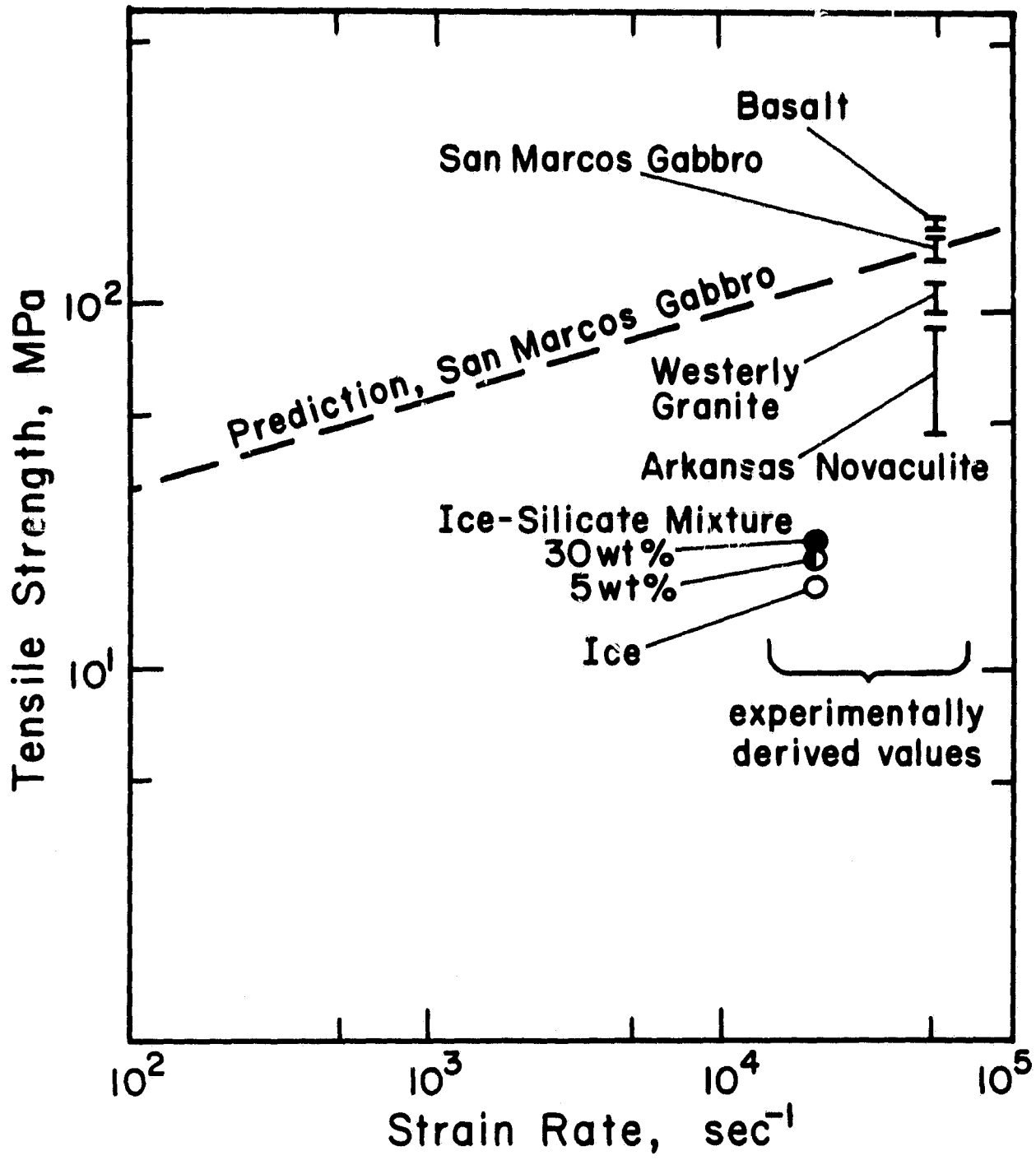

TJA83148SFD

Fig. 9

TJA83149SPH

Fig. 10

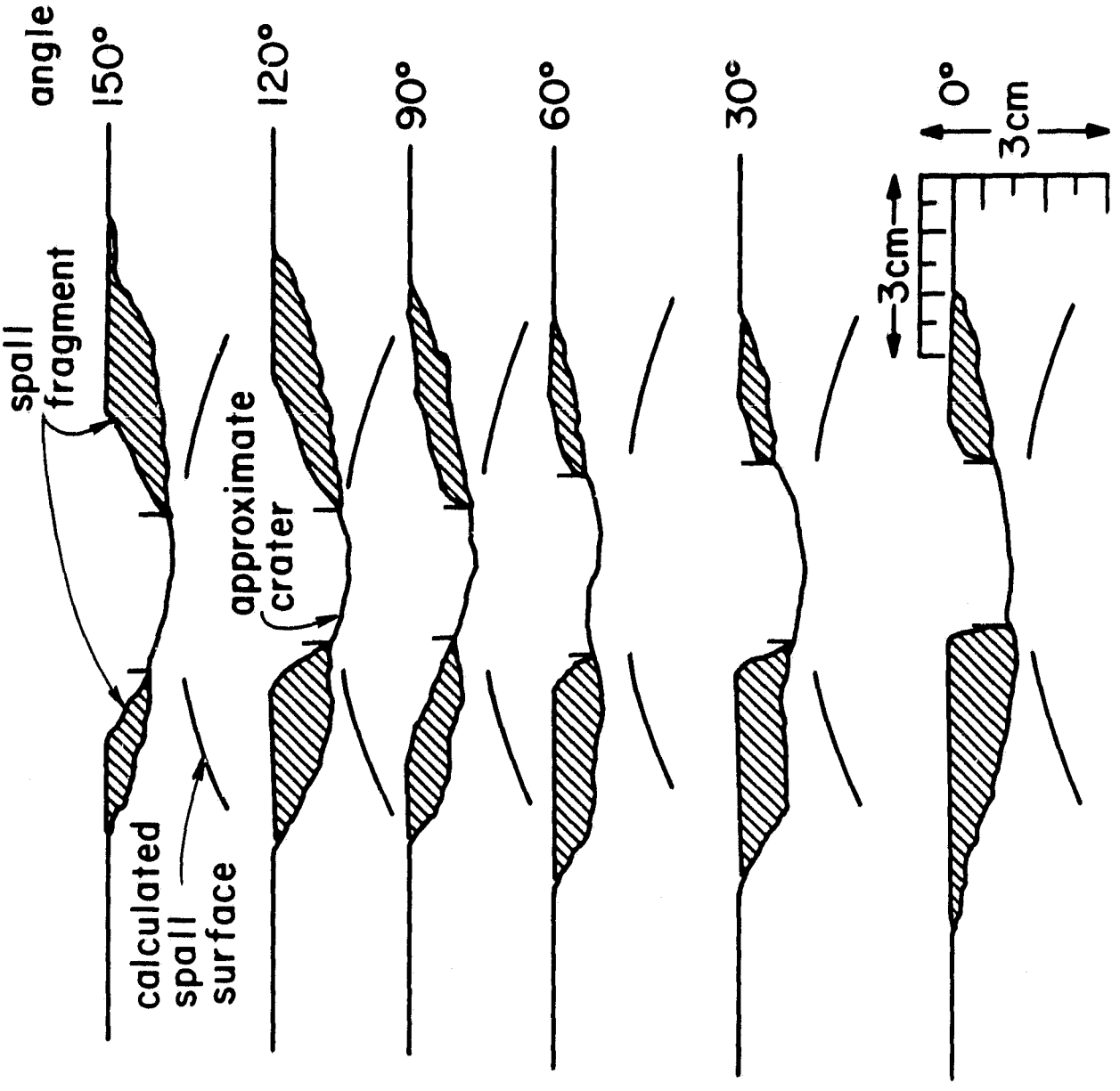

TJA83150SFD

Fig. 11

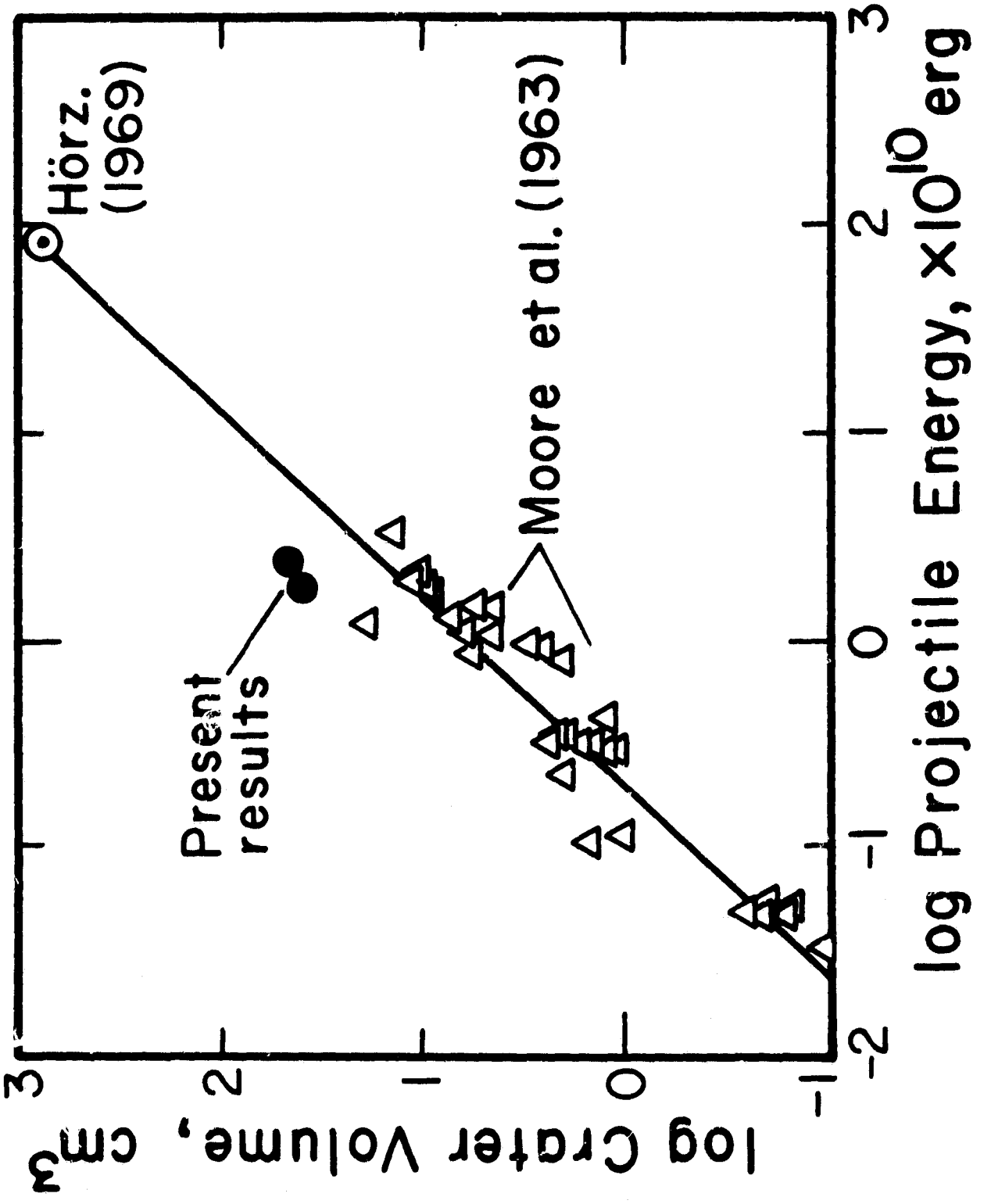

TJA83151SFD

Fig. 12